Journal of Materials Chemistry A RSCPublishing

ARTICLE

The Electronic Structure of Silver Orthophosphate: Experiment and Theory

Cite this: DOI: 10.1039/xoxxoooooox

J.M. Kahk,[a] D. L. Sheridan,[b] A. B. Kehoe,[c] D. O. Scanlon,[d,e] B. J. Morgan,[f] G. W. Watson,[c] and D. J. Payne[a,*]

Received 17th October 2013,
Accepted ooth January 2012

DOI: 10.1039/xoxxoooooox

www.rsc.org/

Since the original discovery of the water-splitting activity of silver orthophosphate (Ag_3PO_4), considerable effort has been devoted to improving its photocatalytic activity and stability through morphology control and the design of multi-component electrode systems. Relatively little attention, however, has been paid to understanding the fundamental electronic properties of this material. Using X-ray photoelectron spectroscopy and hybrid density functional theory (DFT) calculations, we have studied the electronic structure of Ag_3PO_4. Our results indicate that hybrid DFT calculations closely reproduce the structural, electronic, and optical properties of Ag_3PO_4. Further analysis of the experimental and theoretical electronic structure data we have constructed a revised molecular orbital diagram for Ag_3PO_4 that highlights the strong covalent interactions formed in the tetrahedral PO_4 structural units.

Introduction

The search for new materials which can photocatalytically evolve hydrogen and oxygen from water with sunlight, remains a global grand challenge for the scientific community. More than four decades after the first publication of photoelectrochemical (PEC) water splitting using TiO_2,[1] we seem to be no nearer to realizing the full potential of this phenomenon.

Research efforts have focused on TiO_2, but the relatively wide band gap (>3 eV) means this material only absorbs in the UV part of the spectrum, which constitutes only ~5% of the sunlight reaching the earth surface.[2, 3] Materials with smaller band gaps such as Fe_2O_3 (~ 2.1 eV), Cu_2O (2.17 eV) and $BiVO_4$ (2.45 eV) typically suffer from low photoefficiency. For example, $BiVO_4$ displays a quantum yield of only 9% at 450 nm incident light wavelength[4]. Non-oxide semiconductors, which can have high quantum yields, unfortunately suffer from photocorrosion; for example, sulphides and nitrides are prone to self-oxidation in a photoelectrochemical setup.[5, 6] Doping with cations (e.g. V, Mn, or Cr) and anions (e.g. N, S, or P) has also been widely explored as a strategy to improve visible light absorption, with the aim of introducing donor or acceptor levels into the bulk band gap of a host oxide that remains chemically inert. This approach suffers from a loss of performance due to the introduction of numerous recombination centres for the photoexcited charge carriers.[7] It is clear that a more fundamental approach to the design, synthesis, and characterization of water splitting materials is required.

In 2010, it was shown that Ag_3PO_4 displays remarkable photooxidative abilities.[8, 9] It was found that Ag_3PO_4 is more than twice as active as $BiVO_4$ under visible light irradiation, with O_2 production rates of 636 μmol hr^{-1} and 246 μmol hr^{-1} respectively.[9] Remarkable quantum yields of up to 90% have been reported, indicating very low rates of recombination between photoexcited charge carriers. Unfortunately, the conduction band minimum of Ag_3PO_4 is more positive than the H^+/H_2 reduction potential. As a result Ag_3PO_4 will only evolve O_2 and not H_2. A sacrificial reagent such as silver nitrate is also required to be present, to delay the decomposition of the photocatalyst. Therefore, the stability of the photocatalyst remains an issue, which needs to be addressed before commercial application can become viable.

Despite these concerns Ag_3PO_4 has attracted significant research interest following the discovery of its water-splitting properties. Several groups have reported the synthesis and characterization of novel morphologies and composite materials, and many of these exhibit improved photocatalytic activity and stability over bare Ag_3PO_4 powder.[10-19] In addition, Wang et al. have performed electrochemical measurements in conjunction with surface analysis techniques in order to elucidate the mechanism of passivation of Ag_3PO_4 photoelectrodes during the water-splitting reaction.[20]

On the more fundamental side, several groups have used density function theory (DFT) calculations to study the electronic structure of this material.[9, 21-23] As expected, traditional approaches to describing the approximate exchange–correlation potential within DFT, such as the local density

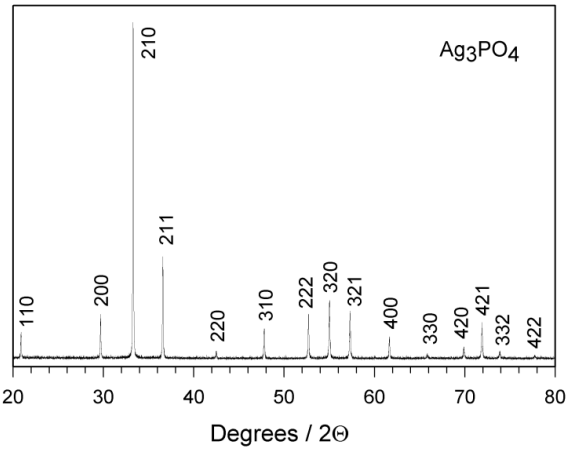

***Figure 1**: An X-ray diffraction pattern of the Ag_3PO_4 powder after refluxing for 24 hours.*

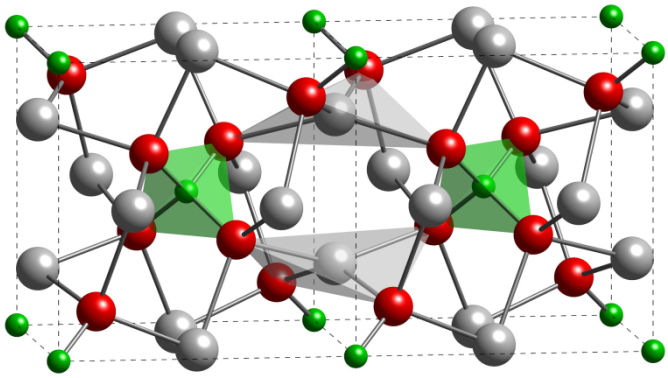

***Figure 2**: The crystal structure of Ag_3PO_4. The local coordination environments of P (tetrahedral) and Ag (distorted tetrahedral) are shown.*

approximation (LDA), lead to a vast underestimation of the magnitude of the band gap due to the self-interaction error inherent to these functionals. To correct for this, two distinct approaches have been used for Ag_3PO_4. Ma et al. and Umezawa et al. have used variants of DFT that incorporate the Hubbard U parameter for the explicit treatment of on-site Coulomb interactions.[21, 22] Liu et al. used a "hybrid" DFT formalism, in which a fixed amount of Fock exchange is added to the base DFT functional.[23] In order that the validity of these earlier calculations can be tested, and the accuracy of future methods could be assessed, experimental characterization of the electronic properties of the material is urgently required.

Here, we present high-resolution X-ray photoelectron spectra of Ag_3PO_4, together with results from theoretical calculations using hybrid DFT. The agreement between the theoretical and experimental results is discussed and it will be shown that hybrid DFT calculations predict the structural, electronic and optical properties of Ag_3PO_4 with good accuracy. In addition, an interpretation of the detailed electronic structure of Ag_3PO_4 from the perspective of molecular orbital (MO) theory is presented.

Experimental section

The Ag_3PO_4 samples were synthesized via a simple precipitation method. 3.0 g $AgNO_3$ and 0.9651 g Na_3PO_4 were dissolved in 100 cm^3 of distilled water. These two solutions were mixed together to form a vibrant yellow precipitate. This was washed through with distilled water, and the resultant powder was dried at 70 C° overnight. With the intent of improving crystallinity, the precipitation method was refined. The two solutions were made up as previously described and mixed in exactly the same way. However, half of the resultant solution was left to digest for 24 hours, and the remaining half was refluxed at 60 C° for 24 hours, both in the dark. The solution left to reflux developed far superior crystallinity. This method was used for the synthesis of further samples.

High-resolution x-ray photoemission spectra of Ag_3PO_4 were measured in a Scienta ESCA 300 spectrometer. This incorporates a rotating anode Al Kα (hν = 1486.6 eV) X-ray source, a 7-crystal X-ray monochromator and a 300 mm mean radius spherical sector electron energy analyser with parallel electron detection system. The X-ray source was run with 200 mA emission current and 14 kV anode bias, whilst the analyser operated at 150 eV pass energy with 0.8 mm slits. Gaussian convolution of the analyser resolution with a linewidth of 260 meV for the X-ray source gives an effective instrument resolution of 400 meV. To negate sample charging the surface charge was stabilised with an electron flood gun delivering 7 eV electrons. Binding energies were referenced to the residual C 1s peak, which was assigned to a binding energy of 284.8 eV.[24] We note that this procedure places the Fermi level ~ 2.1 eV above the top of the valence band, indicating n-type doping in our sample, in agreement with the electrochemical behaviour of Ag_3PO_4 photoelectrodes observed by Yi et al.[9]

Calculation methodology

Calculations were performed using the VASP code,[25] with the projector augmented wave approach[26] used to describe the interaction between the core (Ag:[Kr], P:[Ne], and O:[He]) and the valence electrons. The calculations were performed using the screened hybrid functional proposed by Heyd, Scuseria and Ernzerhof (HSE)[27, 28] in which a percentage (in this case 30%) of exact nonlocal Fock exchange is added to the Perdew, Purke and Ernzerhof functional,[29] with a screening of ω = 0.11 $bohr^{-1}$ applied to partition the Coulomb potential into long range and short range terms. The HSE approach consistently produces structural and band gap data that are more accurate than standard density functional approaches, such as the LDA or GGA.[30-37] A cutoff of 400 eV and a k-point mesh of 3 × 3 × 3 centred on the Γ point were found to be sufficient, and all calculations were deemed to be converged when the forces on all atoms were less than 0.01 eV $Å^{-1}$.

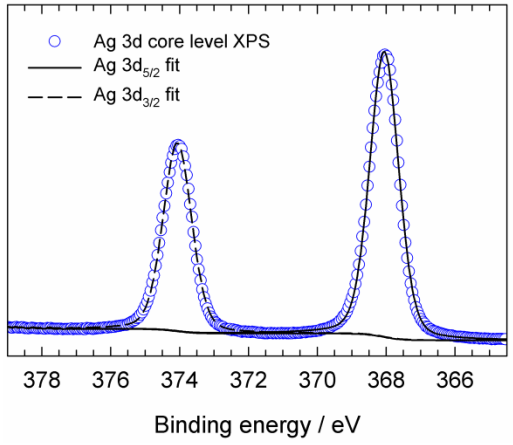

***Figure 3**: The Ag 3d core level region of the photoelectron spectrum fitted using a single symmetric Gaussian-Lorentzian lineshape per peak.*

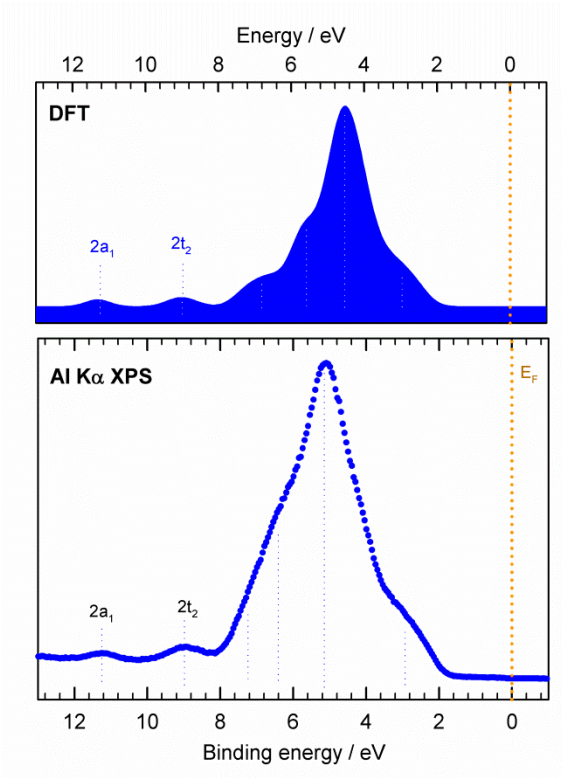

***Figure 4**: A comparison of the valence band region of the photo-electron spectrum (left) and the cross-section weighted calculated density of states with Gaussian broadening applied (right).*

Results and discussion

A diffraction pattern of the as-synthesized Ag_3PO_4 is shown in Figure 1. Highly crystalline Ag_3PO_4 with the cubic structure (space group P4-3N), shown in Figure 2, has been synthesized. The diffraction pattern was indexed using all reflections from 20 to 70˚, and the value of the lattice parameter was determined to be 6.004 Å. The calculated lattice parameter of Ag_3PO_4 obtained from our hybrid DFT calculations is 6.072 Å. For comparison, experimental and calculated lattice parameters from previous studies are listed in Table 1.

Technique	Lattice parameter	Source
Experimental	6.004 Å	This work
Experimental	6.004 Å	Ref [41]
HSE 30	6.072 Å	This work
GGA-PBE LDA-CAPZ	6.113 Å 5.890 Å	Ref. [21]
LDA LDA+U, U(Ag)=4.18 LDA+U, U(Ag)=9.75	5.90 Å 5.88 Å 5.85 Å	Ref. [22]
PBE0	6.010 Å	Ref. [23]

***Table 1:** a comparison of experimental and calculated lattice constants for Ag_3PO_4*

The Ag 3d core levels shown in Figure 3 are easily fitted with one symmetric Gaussian-Lorentzian lineshape per peak, indicating that no measurable reduction of the sample due to exposure to the X-ray beam has occurred. In Figure 4 (top), the theoretical density of states weighted by the photoionization cross-sections and broadened using a Gaussian convolution function is displayed. Good agreement between the experimental and theoretical valence band densities of states is observed, although the binding energy of the feature of highest intensity is underestimated by ~0.5eV in the calculations. This peak is mainly of Ag 4d character, and therefore this slight discrepancy can be attributed to an incorrect cancellation of the self-interaction error in the hybrid DFT approach used. Unusually, this problem cannot be solved by going to higher levels of theory such as the GW approximation,[38] and to date the only possible correction has been the application of an empirical non-local external potential for the d-states, which is fitted to reproduce experimental d-band positions.[39, 40] In this work, we do not artificially augment our calculations with any external potentials, as it will not have a bearing on the generality of our results.

Figure 5(a) shows a band dispersion diagram for Ag_3PO_4 calculated with hybrid DFT, plotted along the high symmetry lines taken from Bradley and Cracknell.[42] The valence band maximum (VBM) is situated at the M point, and is 0.13 eV higher than the highest occupied band at Γ. The conduction band minimum (CBM) is situated at Γ, yielding an indirect fundamental band gap of 2.13 eV, and a direct VBM–CBM bandgap at Γ of 2.26 eV. Experimentally, the indirect and direct band gaps of Ag_3PO_4 have been reported from diffuse reflectance spectroscopy to be 2.36 eV and 2.43 eV respectively.[9]

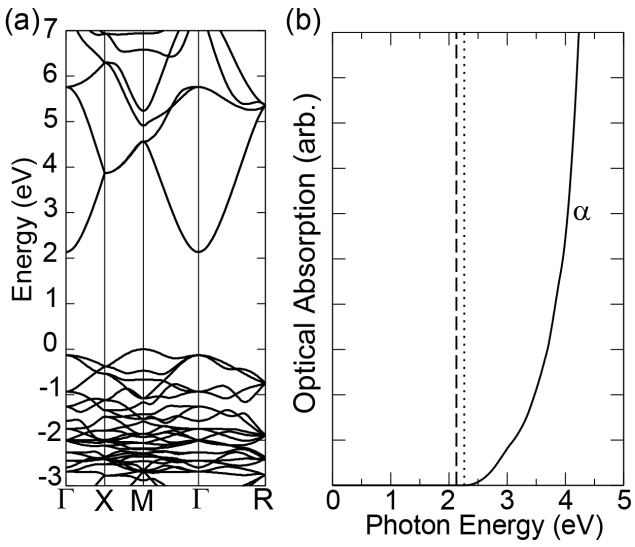

***Figure 5**: (a) A band dispersion diagram for Ag_3PO_4 (b) The optical absorption edge of Ag_3PO_4 calculated using the transversal approximation and PAW method.*

It must be noted, however, that there is a distinct difference between an optical band gap and a fundamental band gap, a point which has been been shown to be extremely important in elucidating the nature of the band gap of In_2O_3,[43] and other important functional oxides.[44-49] To elucidate this further, optical transition matrix elements and the optical absorption spectrum were calculated within the transversal approximation and PAW method.[50] Within this methodology, the adsorption spectra are summed over all direct valence band to conduction band transitions and therefore indirect and intraband adsorptions are ignored.[51] In this framework of single particle transitions, the electron-hole correlations are not treated, and thus would need treatment by higher order electronic structure methods.[52, 53] This method, however, has been previously shown to provide reasonable optical absorption spectra.[44, 54-56]

For Ag_3PO_4, we find that the onset of the optical band gap is 2.26 eV (Figure 5(b)). This onset of absorption corresponds with the direct band gap at the Γ point from the band structure, and calculation of the dipole transition matrix elements between the VB and CB states confirms that the direct optical band gap does indeed occur at the Γ point. Using the Tauc relation, and fitting a slope to the curve, this corresponds to an optical band gap of 2.40 eV, in excellent agreement with the experimental results of Yi et al.[9]

With regards to the physical structure, the valence band electronic structure, and the optical properties of Ag_3PO_4, we further note that our theoretical results are similar to those of the other hybrid calculations,[23] but differ noticeably from those obtained by the LDA+U method, even for the "best" choice of the U parameters.[21, 22] Indeed, it should be emphasized, that the LDA+U correction is a correction that deals with the self-interaction error of the states it is applied to, and should not be used to fit band gaps, except in the case of classical Mott-insulators, where the CBM and VBM are composed of the same orbital.[57] Using a +U correction to fit band gaps can often artificially change the bonding in materials, and can lead to problems when dealing with the electronic structure of defects.[58] In reference [21], the authors also calculate the formation energy and the ionization energy of a silver vacancy (V_{Ag}) in Ag_3PO_4 and suggest that this is the dominant p-type defect and will act as electron recombination

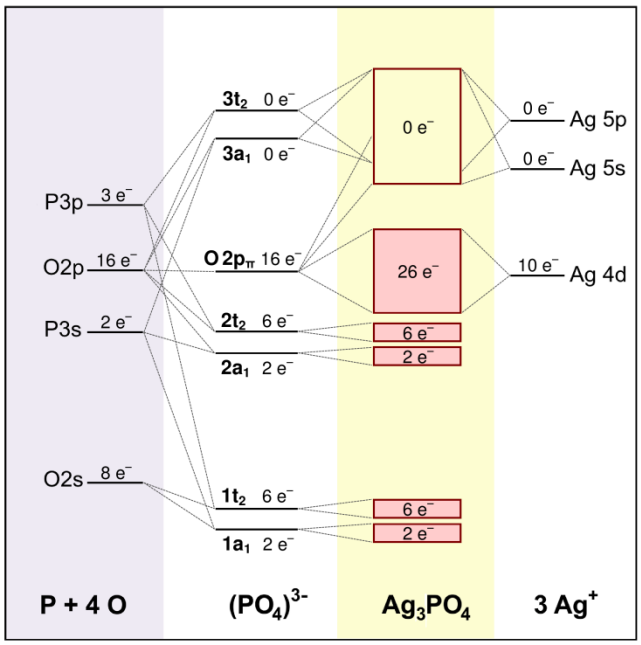

***Figure 6**: A molecular orbital (MO) diagram of Ag_3PO_4.*

centres. Unfortunately, this study predicts that the formation energies of V_{Ag} are in the range -6.5 – -7.5 eV, which would indicate that Ag_3PO_4 is highly unstable with respect to dissociating into Ag metal and phosphate anions. The study also reports that the ionization energy of V_{Ag} calculated using LDA is at 0.46 eV above the VBM, and that the ionization energy calculated using LDA+U is only at 0.12 eV. This is the reverse of what you would expect to happen, as the LDA+U calculations should solve some of the self-interaction error in the system, making the ionization energies deeper, and not shallower.[57, 59, 60] In light of the above, we believe that the LDA+U approach is not suitable for electronic structure calculations of Ag_3PO_4 where an accurate estimate of the band gap and optical absorption properties is required, and that it should therefore be avoided in future work on this material.

The electronic structure of Ag_3PO_4

For transition metal oxides and related materials the electronic structure can often be successfully rationalized in terms of the local coordination environment of the metal atom, using an approach based on molecular orbital (MO) theory. This reflects the highly localized nature of bonding in these materials. For the specific case of Ag_3PO_4, it has been noted

previously that the covalent interactions between the phosphorus and the oxygen atoms are far stronger than those between silver and oxygen.[21] With this in mind, it is possible to construct a molecular orbital diagram for Ag_3PO_4, starting from that of an isolated $(PO_4)^{3-}$ unit.

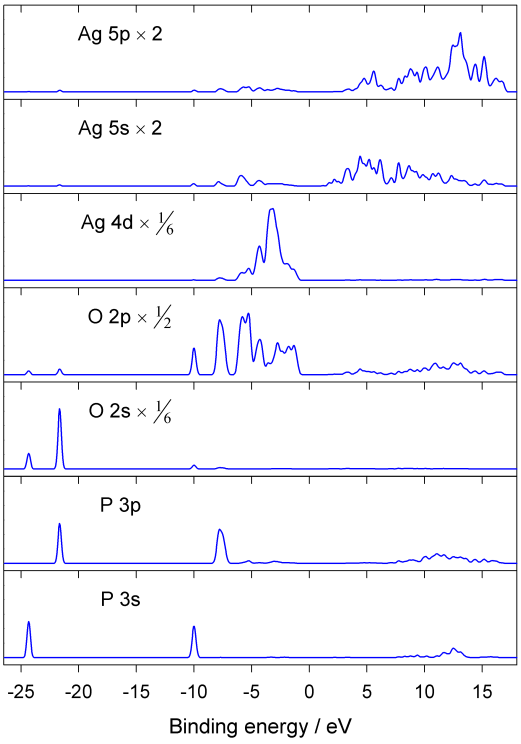

***Figure 7**: Projected densities of states for the Ag 5p, 5s and 4d, O 2p and 2s, and P 3p and 3s orbitals.*

For the $(PO_4)^{3-}$ unit, it is sufficient to consider only sigma interactions between the orbitals on P and O. The four oxygen atoms contribute two orbitals of sigma symmetry each: the 2s, and one of the three 2p. Under a tetrahedral environment these yield two triply degenerate ligand group orbitals (LGOs) of t_2 symmetry, and two LGOs of a_1 symmetry. These overlap with the P 3s (a_1), and P 3p (t_2) orbitals to form twelve molecular orbitals (MOs) as shown in Figure 6. The features of the MO diagram of the $(PO_4)^{3-}$ unit are clearly identifiable in the partial density of states plots obtained from our hybrid DFT calculations shown in Figure 7. In particular, the $1a_1$, $1t_2$, $2a_1$ and $2t_2$ orbitals are visible at 25.7 eV, 23.0 eV, 11.3 eV and 9.0 eV respectively. Notably, the P 3p orbitals only contribute to the states with t_2 symmetry, whilst the P 3s orbitals only contribute to states with a_1 symmetry. We further note that the $2a_1$ and $2t_2$ orbitals are also clearly visible as distinct states at the bottom of the valence band in the photoelectron spectrum of Ag_3PO_4 (Figure 4). In contrast, the $3a_1$ and $3t_2$ orbitals are not identifiable as distinct states, but are instead strongly hybridized with Ag 5s and 5p orbitals and contribute towards the part of the conduction band more than 5 eV above the Fermi level.

The rest of the O 2p orbitals, with π symmetry with respect to the $(PO_4)^{3-}$ tetrahedron, and to a lesser extent also the $2a_1$ and $2t_2$ orbital, mix with the Ag 4d orbitals to form the states in the upper part of the valence band. We note that the band formed by the Ag 4d states extends over ~ 6 eV, indicating that

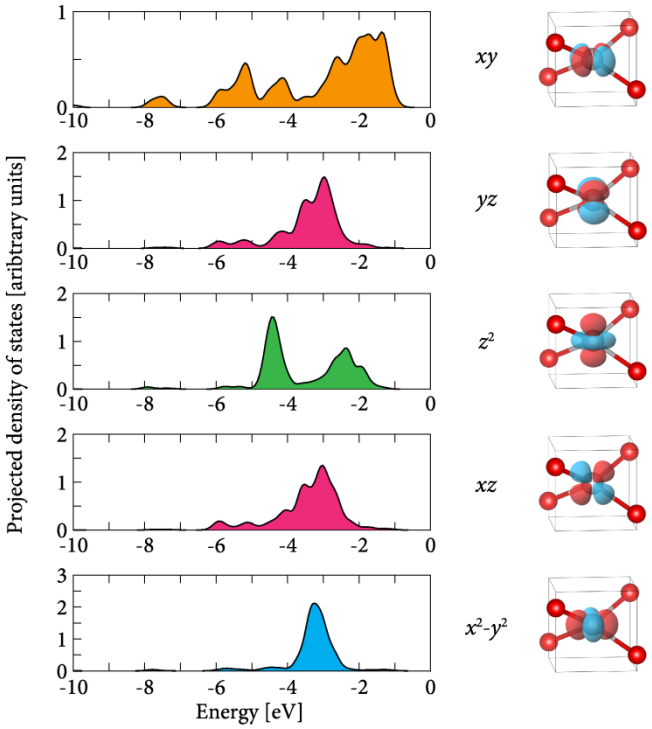

***Figure 8**: Projected densities of states for the individual Ag 4d components.*

hybridization between the O 2p and Ag 4d states is certainly not negligible, unlike what was postulated in reference [22]. Upon taking a closer look at the individual Ag 4d orbitals, shown in Figure 9, it becomes evident that the d_{xy} orbitals that point towards the ligands exhibit the strongest mixing with O 2p based states, whilst the d_{x2-y2} orbitals that point between the ligands remain largely non-bonding. The d_{z2}, d_{xz} and d_{yz} orbitals are intermediate in character.

These considerations allow us to construct a schematic diagram for bonding in Ag_3PO_4. At this point it should be noted that construction of an MO diagram for Ag_3PO_4 has been attempted previously by Ma et al,[21] but the states near the bottom of the valence band have been incorrectly described as being P-O p π-bonding, and the lowest energy state corresponding to the $(PO_4)^{3-}$ $1a_1$ orbital has been incorrectly described as having strong O2p and no O 2s character. Furthermore, the upper part of the valence band has been described as consisting of non-interacting Ag 4d and O 2p – π orbitals, at odds with our, and previous calculations for this

material. A revised and complete MO diagram for Ag_3PO_4 is shown in Figure 6.

Finally, it is worthwhile to consider why Ag_3PO_4 exhibits higher photocatalytic activity than other Ag(I) materials, such as Ag_2O. In reference [22], it was argued that the difference can be ascribed to intrinsically better carrier mobility in Ag_3PO_4, arising from the conduction band in Ag_3PO_4 having less Ag 4d character than the conduction band of Ag_2O. This in turn was explained with reference to the claim that hybridization between the Ag 4d and O 2p orbitals in Ag_3PO_4 is very weak. To elucidate this issue further, we have evaluated the charge distribution in the two materials by performing a Bader analysis. The results are for Ag_3PO_4: Ag = 0.70, P = 3.82, O = -1.48 and for Ag_2O: Ag = 0.52, O = -1.04. It is clear that the partial positive charge on the Ag atoms in Ag_3PO_4 is greater than in Ag_2O leading to a preferential stabilization of the poorly penetrating Ag 4d orbitals and a consequent widening of the Ag 4d – Ag 5s gap. This is likely to be an additional contributor for why the filled Ag 4d orbitals are less strongly hybridized with the empty levels near the bottom of the conduction band in Ag_3PO_4. It should however be noted, that according to previous electronic structure calculations, the bands contributing to the CBM in Ag_2O are nevertheless highly dispersive, and it is not clear, why the presence of Ag 4d character in itself should lead to lower carrier mobility. Instead we tentatively propose that the differences in photocatalytic performance between these two materials may be primarily due to differences in their defect chemistries. Indeed, recent theoretical work suggests that intrinsic point defects in Ag_3PO_4 are unlikely to behave as recombination centres for excited charge carriers, and that the formation energy of oxygen vacancies in Ag_3PO_4 is high due to the high stability of the $(PO_4)^{3-}$ units.[61] To elucidate this issue further, and improve our general understanding of the catalytic behaviour of Ag_3PO_4, additional experimental studies of the fundamental bulk and surface properties of Ag_3PO_4 are required.

Conclusions

In summary, we have used photoelectron spectroscopy and density functional theory calculations to study the electronic structure of Ag_3PO_4. We have found that calculations within the hybrid DFT framework yield an accurate representation of the electronic, structural, and optical properties of Ag_3PO_4, and should therefore be preferred over LDA+U based approaches for future work. Aligning the photoemission data using a reference value for the carbon 1s peak originating from the surface contamination layer places the Fermi level of our sample near the bottom of the conduction band. This indicates weak n-type doping, in agreement with Yi et al.[9] Additionally, our analysis of the valence band electronic structure of Ag_3PO_4 shows that it is dominated by the strong bonding interactions in the tetrahedral $(PO_4)^{3-}$ units. Narrow bands derived from the $2a_1$ and $2t_2$ orbitals of an isolated $(PO_4)^{3-}$ unit are easily identifiable in the experimental photoelectron spectrum below the bottom of the valence band. We also find clear evidence for hybridization between the Ag 4d and O 2p states in Ag_3PO_4, and the splitting of the Ag 4d levels can be rationalized in terms of their local coordination environment of D_{2d} symmetry.

Acknowledgements

We would like to thank Professor Russell Egdell and Professor Louis Piper for very helpful discussions. D. J. P. acknowledges support from the Royal Society (UF100105). J. M. K. acknowledges support from EPSRC for a Doctoral Prize Studentship. D. J. P. and D. O. S. acknowledge the support of the Materials Design Network. The work in TCD was supported by SFI through the PI programme (PI Grant numbers 06/IN.1/I92 and 06/IN.1/I92/EC07). Calculations were performed on the Kelvin and Lonsdale supercomputers as maintained by TCHPC. B. J. M. acknowledges support from EPSRC grant ref. EP/H003819/1.

Notes and references

[a] Department of Materials, Imperial College London, Exhibition Road, London SW7 2AZ, UK.

[b] Department of Chemistry, University of Oxford,Chemistry Research Laboratory, 12 Mansfield Road, Oxford, OX1 3TA, UK.

[c] School of Chemistry and CRANN, Trinity College Dublin, Dublin 2, Ireland.

[d] University College London, Kathleen Lonsdale Materials Chemistry, Department of Chemistry, 20 Gordon Street, London WC1H 0AJ, UK

[e] Diamond Light Source Ltd., Diamond House, Harwell Science and Innovation Campus, Didcot, Oxfordshire OX11 0DE, UK

[f] Department of Materials, University of Oxford, Parks Road, OX1 3PH, U.K.

1. Fujishima, A. and K. Honda, Nature, 1972. **238**: p. 37.
2. Hashimoto, K., H. Irie, and A. Fujishima, *TiO2 photocatalysis: A historical overview and future prospects.* Japanese Journal of Applied Physics Part 1-Regular Papers Brief Communications & Review Papers, 2005. **44**(12): p. 8269-8285.
3. Scanlon, D.O., et al., *Band alignment of rutile and anatase TiO2.* Nature Materials, 2013. **12**(9): p. 798-801.
4. Kudo, A., K. Omori, and H. Kato, *A novel aqueous process for preparation of crystal form-controlled and highly crystalline BiVO4 powder from layered vanadates at room temperature and its photocatalytic and photophysical properties.* Journal of the American Chemical Society, 1999. **121**(49): p. 11459-11467.
5. Osterloh, F.E., *Inorganic Materials as Catalysts for Photoelectrochemical Splitting of Water.* Chem. Mater., 2008. **20**: p. 35.
6. Osterloh, F.E., *Inorganic nanostructures for photoelectrochemical and photocatalytic water splitting.* Chemical Society Reviews, 2013. **42**(6): p. 2294-2320.
7. Henderson, M.A., *A surface science perspective on TiO2 photocatalysis.* Surface Science Reports, 2011. **66**(6-7): p. 185-297.
8. Yi, Z., R.L. Withers, and Y. Liu, *A two-step approach towards solar-driven water splitting.* Electrochemistry Communications, 2010: p. in press.
9. Yi, Z.G., et al., *An orthophosphate semiconductor with photooxidation properties under visible-light irradiation.* Nature Materials, 2010. **9**(7): p. 559-564.
10. Cao, J., et al., *Visible light photocatalytic activity enhancement and mechanism of AgBr/Ag3PO4 hybrids for degradation of methyl orange.* Journal of Hazardous Materials, 2012. **217**: p. 107-115.
11. Liu, W., et al., *Ag3PO4/ZnO: An efficient visible-light-sensitized composite with its application in photocatalytic degradation of*

Rhodamine B. Materials Research Bulletin, 2013. **48**(1): p. 106-113.
12. Zhu, M.S., P.L. Chen, and M.H. Liu, *Visible-light-driven Ag/Ag3PO4-based plasmonic photocatalysts: Enhanced photocatalytic performance by hybridization with graphene oxide.* Chinese Science Bulletin, 2013. **58**(1): p. 84-91.
13. Jiang, B.J., et al., *InSitu Fabrication of Ag/Ag3PO4/Graphene Triple Heterostructure Visible-Light Photocatalyst through Graphene-Assisted Reduction Strategy.* Chemcatchem, 2013. **5**(6): p. 1359-1367.
14. Bi, Y.P., et al., *Photocatalytic and photoelectric properties of cubic Ag3PO4 sub-microcrystals with sharp corners and edges.* Chemical Communications, 2012. **48**(31): p. 3748-3750.
15. Wang, Y.F., et al., *Novel visible-light AgBr/Ag3PO4 hybrids photocatalysts with surface plasma resonance effects.* Journal of Solid State Chemistry, 2013. **202**: p. 51-56.
16. Lin, H.L., et al., *Ag3PO4 quantum dot sensitized BiPO4: A novel p-n junction Ag3PO4/BiPO4 with enhanced visible-light photocatalytic activity.* Catalysis Communications, 2013. **37**: p. 55-59.
17. Bi, Y., et al., *Facet Effect of Single-Crystalline Ag3PO4 Sub-microcrystals on Photocatalytic Properties.* Journal of the American Chemical Society, 2011. **133**(17): p. 6490-6492.
18. Yao, W.F., et al., *Synthesis and characterization of high efficiency and stable Ag3PO4/TiO2 visible light photocatalyst for the degradation of methylene blue and rhodamine B solutions.* Journal of Materials Chemistry, 2012. **22**(9): p. 4050-4055.
19. Rawal, S.B., S.D. Sung, and W.I. Lee, *Novel Ag3PO4/TiO2 composites for efficient decomposition of gaseous 2-propanol under visible-light irradiation.* Catalysis Communications, 2012. **17**: p. 131-135.
20. Wang, W.G., et al., *Visible-Light Photocatalytic Activity and Deactivation Mechanism of Ag3PO4 Spherical Particles.* Chemistry-an Asian Journal, 2012. **7**(8): p. 1902-1908.
21. Ma, X.G., et al., *Origin of Photocatalytic Activation of Silver Orthophosphate from First-Principles.* Journal of Physical Chemistry C, 2011. **115**(11): p. 4680-4687.
22. Umezawa, N., O.Y. Shuxin, and J.H. Ye, *Theoretical study of high photocatalytic performance of Ag3PO4.* Physical Review B, 2011. **83**(3).
23. Liu, J.J., et al., *Electronic structure and optical properties of Ag3PO4 photocatalyst calculated by hybrid density functional method.* Applied Physics Letters, 2011. **99**(19).
24. Miller, D.J., M.C. Biesinger, and N.S. McIntyre, *Interactions of CO2 and CO at fractional atmosphere pressures with iron and iron oxide surfaces: one possible mechanism for surface contamination?* Surface and Interface Analysis, 2002. **33**(4): p. 299-305.
25. Kresse, G. and J. Furthmüller, Phys. Rev. B, 1996. **54**: p. 11169.
26. Kresse, G. and D. Joubert, *From ultrasoft pseudopotentials to the projector augmented-wave method.* Physical Review B, 1999. **59**(3): p. 1758-1775.
27. Heyd, J., G.E. Scuseria, and M. Ernzerhof, J. Chem. Phys., 2003. **118**: p. 8207.
28. Krukau, A.V., et al., *Influence of the exchange screening parameter on the performance of screened hybrid functionals.* Journal of Chemical Physics, 2006. **125**(22).
29. Perdew, J.P., K. Burke, and M. Ernzerhof, *Generalized gradient approximation made simple.* Phys. Rev. Lett., 1996. **77**(18): p. 3865.
30. Heyd, J. and G.E. Scuseria, J. Chem. Phys., 2004. **121**: p. 1187.
31. Heyd, J., et al., *Energy band gaps and lattice parameters evaluated with the Heyd-Scuseria-Ernzerhof screened hybrid functional.* Journal of Chemical Physics, 2005. **123**(17).
32. Scanlon, D.O., et al., *Acceptor Levels in p-Type Cu2O: Rationalizing Theory and Experiment.* Physical Review Letters, 2009. **103**(9).
33. Scanlon, D.O. and G.W. Watson, *(Cu2S2)(Sr3SC2O5)-A Layered, Direct Band Gap, p-Type Transparent Conducting Oxychalcogenide: A Theoretical Analysis.* Chemistry of Materials, 2009. **21**(22): p. 5435-5442.
34. Scanlon, D.O., A. Walsh, and G.W. Watson, *Understanding the p-Type Conduction Properties of the Transparent Conducting Oxide CuBO2: A Density Functional Theory Analysis.* Chemistry of Materials, 2009. **21**(19): p. 4568-4576.
35. Allen, J.P., D.O. Scanlon, and G.W. Watson, *Electronic structure of mixed-valence silver oxide AgO from hybrid density-functional theory.* Physical Review B, 2010. **81**(16).
36. Stroppa, A. and G. Kresse, *Unraveling the Jahn-Teller effect in Mn-doped GaN using the Heyd-Scuseria-Ernzerhof hybrid functional.* Physical Review B, 2009. **79**(20).
37. Stroppa, A. and S. Picozzi, *Hybrid functional study of proper and improper multiferroics.* Physical Chemistry Chemical Physics, 2010. **12**(20): p. 5405-5416.
38. Lim, L.Y., et al., *Angle-resolved photoemission and quasiparticle calculation of ZnO: The need for d band shift in oxide semiconductors.* Physical Review B, 2012. **86**(23).
39. Lany, S., *Band-structure calculations for the 3d transition metal oxides in GW.* Physical Review B, 2013. **87**(8).
40. Peng, H.W., et al., *Convergence of density and hybrid functional defect calculations for compound semiconductors.* Physical Review B, 2013. **88**(11).
41. Ng, H.N., C. Calvo, and R. Faggiani, *New Investigation of Structure of Silver Ortho-Phosphate.* Acta Crystallographica Section B-Structural Science, 1978. **34**(Mar): p. 898-899.
42. Bradley, C.J. and A.P. Cracknell, *Mathematical Theory of Symmetry in Solids*. 1972: Oxford University Press.
43. Walsh, A., et al., *The nature of the bandgap in In2O3 revealed by first-principles calculations and X-ray spectroscopy.* Phys. Rev. Lett., 2008. **100**: p. 167402.
44. Nie, X.L., S.H. Wei, and S.B. Zhang, *Bipolar doping and band-gap anomalies in delafossite transparent conductive oxides.* Phys. Rev. Lett., 2002. **88**(6): p. 066405.
45. Godinho, K.G., et al., *Understanding conductivity in SrCu2O2: stability, geometry and electronic structure of intrinsic defects from first principles.* Journal of Materials Chemistry, 2010. **20**(6): p. 1086-1096.
46. Dahl, J.P. and A.C. Switendick, J. Phys. Chem. Solids, 1966. **27**.
47. Frohlich, D., R. Kenklies, and R. Helbig, *Band-Gap Assignment in Sno2 by 2-Photon Spectroscopy.* Phys. Rev. Lett., 1978. **41**(25): p. 1750.
48. Stapelbroek, M. and B.D. Evans, *Exciton Structure in Uv-Absorption Edge of Tetragonal Geo2.* Solid State Communications, 1978. **25**(11): p. 959-962.
49. Segev, D. and S.H. Wei, *Structure-derived electronic and optical properties of transparent conducting oxides.* Phys. Rev. B, 2005. **71**(12): p. 125129.
50. Gajdos, M., et al., *Linear optical properties in the projector-augmented wave methodology.* Physical Review B, 2006. **73**(4).
51. Adolph, B., J. Furthmuller, and F. Bechstedt, *Optical properties of semiconductors using projector-augmented waves.* Physical Review B, 2001. **63**(12): p. art. no.-125108.
52. Ramos, L.E., et al., *Optical spectra of Si nanocrystallites: Bethe-Salpeter approach versus time-dependent density-functional theory.* Physical Review B, 2008. **78**(19).
53. Paier, J., M. Marsman, and G. Kresse, *Dielectric properties and excitons for extended systems from hybrid functionals.* Physical Review B, 2008. **78**(12).
54. Walsh, A., et al., Phys. Rev. B, 2009. **79**: p. 073105.
55. Huda, M.N., et al., *Group-IIIA versus IIIB delafossites: Electronic structure study.* Physical Review B, 2009. **80**(3).
56. Scanlon, D.O. and G.W. Watson, *Band gap anomalies of the (ZnM2O4)-O-III (M-III = Co, Rh, Ir) spinels.* Physical Chemistry Chemical Physics, 2011. **13**(20): p. 9667-9675.
57. Morgan, B.J., D.O. Scanlon, and G.W. Watson, e J. Surf. Sci. Nano Tech., 2009. **7**.
58. Laubach, S., et al., *Theoretical and experimental determination of the electronic structure of V2O5, reduced V2O5-x and sodium intercalated NaV2O5.* Physical Chemistry Chemical Physics, 2007. **9**(20): p. 2564-2576.
59. Raebiger, H., S. Lany, and A. Zunger, *Origins of the p-type nature and cation deficiency in Cu2O and related materials.* Phys. Rev. B, 2007. **76**: p. 045209.
60. Scanlon, D.O., B.J. Morgan, and G.W. Watson, *Modeling the polaronic nature of p-type defects in Cu2O: The failure of GGA and GGA plus U.* Journal of Chemical Physics, 2009. **131**(12).

61. Reunchan, P. and N. Umezawa, *Native defects and hydrogen impurities in Ag3PO4.* Physical Review B, 2013. **87**(24).

